Voipio, Veli E.

GPR pulse propagation topography

Published in:
Applied Computational Electromagnetics Society Journal

Published: 01/05/2021

Document Version
Publisher's PDF, also known as Version of record

Please cite the original version:
Voipio, V. E. (2021). GPR pulse propagation topography. *Applied Computational Electromagnetics Society Journal*, *36*(5), 596-602. https://aces-society.org/includes/downloadpaper.php?of=ACES_Journal_May_2021_Paper_14&nf=21-5-14

GPR Pulse Propagation Topography

Veli E. Voipio

Department of Electronics and Nanoengineering, School of Electrical Engineering
Aalto University, Espoo, P.O. Box 11000, FI-00076 AALTO, FINLAND
veli-erkki.voipio@aalto.fi

Abstract — In this article, I propose a new method for calculating and visualizing the pulse radiation within the depth range commonly used by Ground Penetrating Radar (GPR). The text describes the method and illustrates the propagation with several examples. One conventional method is also applied for a quick comparison. The method can be used to optimize GPR antennas and transmit pulse shapes.

Index Terms — Antennas, FDTD, Ground Penetrating Radar (GPR), patch antenna, propagation, UWB.

I. INTRODUCTION

When using Ground Penetrating Radar (GPR), it is important to know the pulse propagation behavior in the range normally used by GPR. Both the antenna design and the excitation pulse shape affect the radar performance. The proposed method relates to recent research: [1] describes what they call "near field directivity"; [2] uses near field distribution; [3] shows single-frequency far field patterns in dielectric half-space and also discusses the antenna footprint approximation; the total (received pulse) energy concept is used in [4] and [5]; pulse radiation visualizations also exist, e.g., in [6]; ongoing pulse shape research is suggested in [7].

The GPR range is roughly twenty wavelengths downwards into the medium [1]. The radiated field behavior is not trivial that close to the antenna. The antenna and target size and the depth are all of similar magnitude. The wide spectrum means that at a specific point the reactive near field, diffractive (Fresnel) and far field (Fraunhofer) exist simultaneously at various frequencies. [3] mentions: "Near the antennas the fields are more complex and require numerical simulation". According to [7], the GPR radiation patterns do not exhibit far-field behavior. Summing up, new analysis methods should be explored.

In this article, I introduce a new method to calculate the radiation in the ground and to visualize it: the peak amplitude of the simulated pulse (maximal magnitude of the electric field passing the point/pixel/voxel) is stored. That information can be used to create a map of the radiation: a quantitative radiation topography, and it is available for various kinds of postprocessing.

No similar method exists so far to my knowledge, but my method visually resembles those where the contours show color as path loss at height and distance points in the radio propagation, revealing ducting and other possible features [8]. Simulations for the fields near the antenna in the ground have been available for decades, but this kind of calculation of the maximal field value in each point is new. It allows quick estimation of the propagation, although the time and frequency information are lost. One can expect that this calculation method adds a new variable for the research and design: it provides important information to improve the GPR antennas, optimize the transmit pulse, and for the tomography/inverse processing.

The paper is organized as follows. Section II describes the new method. In Section III, there are examples of the calculations, comparing the Gopher antenna [9] with a loaded dipole model. Section IV shows examples for a combined schematic pattern of a bistatic radar antenna. Section V illustrates the effect of the pulse width on radiation topography. Section VI presents conventional pulse radiation solutions applied to the GPR range, and Section VII the far field radiation pattern for comparison. Section VIII discusses a field measurement example. Section IX concludes the article with an evaluation.

II. THE METHOD

The Finite-Difference Time-Domain (FDTD) method with a Gaussian pulse is commonly applied to indicate the wideband spectrum and phase behavior of the electromagnetic waves. Now I am proposing a procedure that stores the highest electric field magnitude (combination of all three field components) during the FDTD simulation in each pixel in a defined plane. As time passes in the FDTD simulation with Gaussian pulse excitation, at each time step in each cell or voxel the field strength is compared to the maximum thus far encountered. If larger, then it becomes the new maximal value. The maximal field strengths in the maps do not occur at the same instant of time. One must interpret it the same way as ducting is visualized in [8]. Commercial and

Submitted On: January 15, 2021
Accepted On: April 18, 2021

https://doi.org/10.47037/2020.ACES.J.360514

academic FDTD codes are available, also for GPR, for example [10] but they cannot be modified by the users. Thus, I have modified the code in [11] for the FDTD simulation. The result can be visualized and used for postprocessing. However, this visualization method does not inform about the time, phase and propagation direction of the signal. Nevertheless, the explorative expectation is that the pulse shape stays reasonably similar in the area of interest. This expectation is evaluated in Section IX.

The Gopher antenna structure in Fig. 1 was used in the simulations. The Gopher antenna is described in [9]. The spacing between the Gopher antenna pair is 100 mm. For comparison, a loaded center-fed wire dipole is defined here as a reasonable representative corresponding to the common commercial loaded dipoles. The dipole used for the comparison is 450 mm long and the dipole pair spacing is 120 mm. The material has a conductivity of 30 S/m in order to achieve a sufficient bandwidth using the low conductivity as an evenly distributed resistive load.

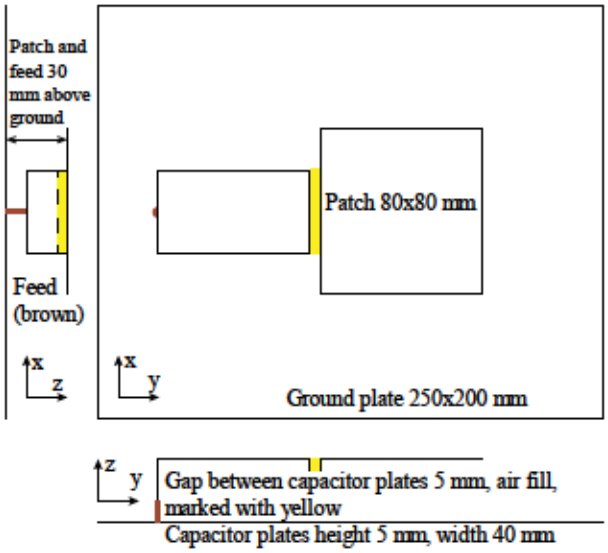

Fig. 1. Gopher antenna structure drawing with dimensions. Material is copper plate 0.5 mm. In FDTD simulations, the perfect electric conductor was used as material.

In this study, the Gopher antenna is filled with neoprene, $\varepsilon_r = 6.7$ to lower the central frequency of the antenna and to improve the matching to the ground (commonly $\varepsilon_r = 6$–8 in the ground). Both the dipole and the Gopher antennas have a wide spectrum and a good Gaussian pulse response: the central frequency of the Gopher antenna with the neoprene fill is 440 MHz, and the spectrum with the -10 dB of the maximal power limit is 220–630 MHz. The central frequency of the loaded dipole antenna is 300 MHz and the spectrum with the -10 dB of the maximal power limit is 120–630 MHz. The simulations in Sections III and IV use a Gaussian pulse. The pulse is 1.4 ns at 50% of the maximal amplitude. In order to have the same transmit power in both antennas, the excitation voltage is 1 V for the Gopher antenna, and 3.4 V for the loaded dipole.

The simulated ground volume is 600 mm deep with an 800x800 mm^2 footprint, using 5 mm voxels. Antennas are 20 mm above the ground, as [7] concurs. The permittivity $\varepsilon_r = 6.7$ is used in the ground. The simulation space above the ground is air and contains two identical antennas in each simulation: either Gopher or dipole antennas.

The absorbing boundary is convolutional perfectly matched layer (CPML) as in [11], but the simulation space is in direct contact with the CPML, without the air gap between. The time step is calculated in the code resulting $\Delta t = 8.7$ picoseconds. That is optimal for the air although oversampling in neoprene. If ten times the distance between two grid points (10·5 mm = 50 mm) is used to define the minimal wavelength in one dimension [12], then the minimal wavelength $\lambda_{min} = \sqrt{3} \cdot 50$ mm = 87 mm in a cube in air. Then the maximal frequency when the FDTD grid is valid $f_{max} = c/(\lambda_{min} \cdot \sqrt{\varepsilon_r}) = 1.3$ GHz.

All the simulations have two antennas in the simulation space, except the simulations used to create Fig. 15. The simulation spaces are shown in Fig. 3 and Fig. 4. An enlargement of the simulation space in the yz-plane is in Fig. 2. showing the antenna section and the neoprene fill in and around it.

Fig. 2. Gopher antenna in the simulation space, yz-plane, showing the neoprene fill around the antenna and in the ground in gray. The gap between the antenna and the ground is 20 mm.

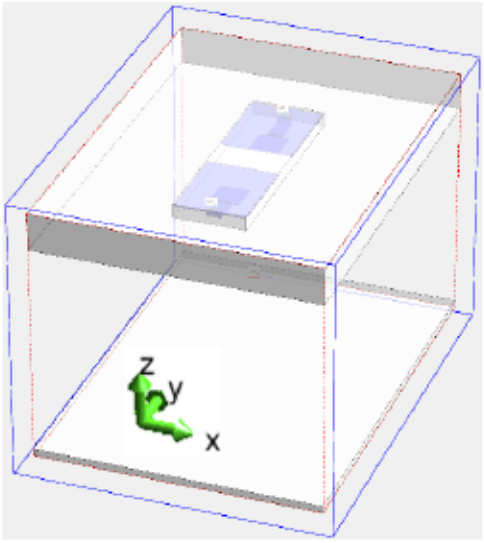

Fig. 3. Gopher antenna simulation space. Two antennas side-by-side, 100 mm gap between them. Xz-plane is in the middle of the gap parallel to the short edges of the antennas, and yz-plane goes through the centers of the antennas.

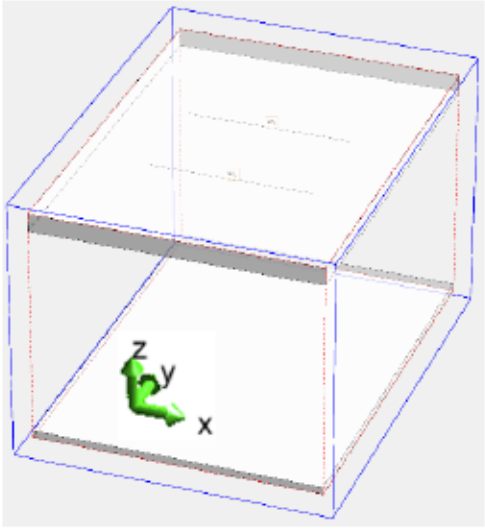

Fig. 4. Dipole antenna simulation space. Two antennas side-by-side, 120 mm gap between them. Xz-plane is in the middle of the gap parallel to the antennas, and yz-plane goes across the centers of the antennas.

III. GOPHER ANTENNA AND LOADED DIPOLE RADIATION

The calculation results illustrated in Fig. 5 and Fig. 6 show the electric field maximal magnitude with the 1.4 ns transmit pulse in the yz plane. The yz plane is electrically the E-plane for the Gopher antenna, and H-plane for the dipole. The colorbar is in dB and 0 dB is 6 V/m in all pictures 5–12.

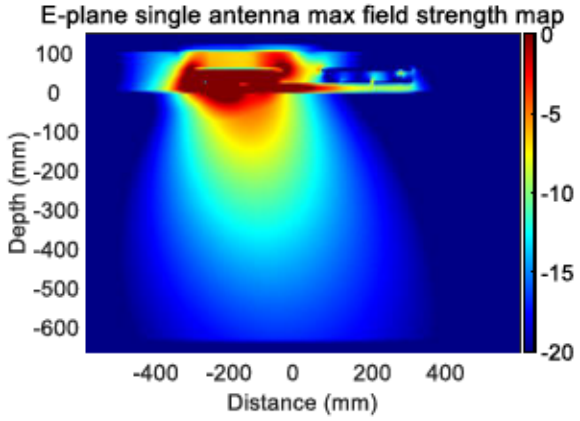

Fig. 5. Gopher antenna yz-plane (E-plane) max field strength map by a 1.4 ns transmit pulse, through the antenna centers.

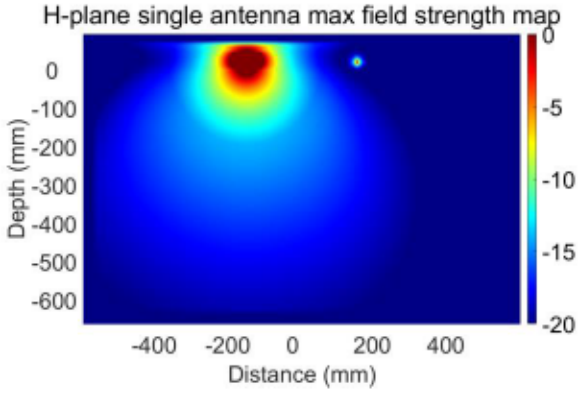

Fig. 6. Dipole antenna yz-plane (H-plane) max field strength map by a 1.4 ns transmit pulse, through the antenna centers.

Below Fig. 7 and Fig. 8 show the electric field maximal magnitude in the xz plane between the antenna pair.

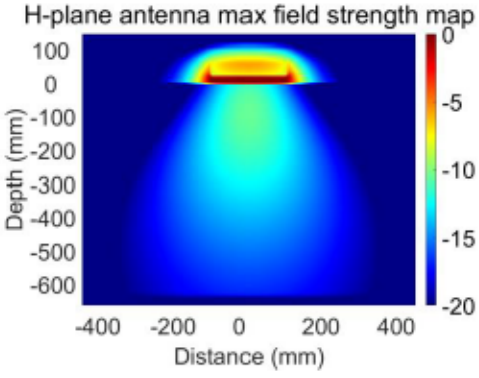

Fig. 7. Gopher antenna xz-plane (H-plane) max field strength map by a 1.4 ns transmit pulse, through the antenna centers.

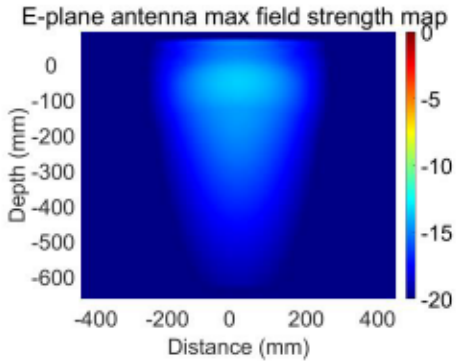

Fig. 8. Dipole antenna xz-plane (E-plane) max field strength map by a 1.4 ns transmit pulse, through the antenna centers.

IV. EXAMPLES OF A COMBINED PATTERN

In a monostatic radar, the gain is the square of the antenna gain. In a bistatic radar, the case is more complex. Here I approximate the combined radiation topography by multiplying the transmit and receiver antenna radiation values at each point (voxel). Figure 9 and Fig. 10 show the results, and they can be compared with Fig. 5 and Fig. 6, respectively.

Comparable cases are very rare in the literature. For the dipole, one comparable case is in [5] (design information in [13]), where the 6 dB beam (two-way gain, corresponds to the 3 dB beam in my simulation) is 75° wide in materials with $\varepsilon_r = 5$ and 10. In my simulation the dipole antenna pair 3 dB beam is 80° wide, as inferred from Fig. 10 at the 600 mm depth.

Another comparable case is in [1] where the E-plane dipole pair beam at 11 ns travel distance in oil ($\varepsilon_r = 2.1$) is 38° wide (my estimation from the picture, assuming the picture represents received power from two-way travel). In my simulation the corresponding beam is 32° wide.

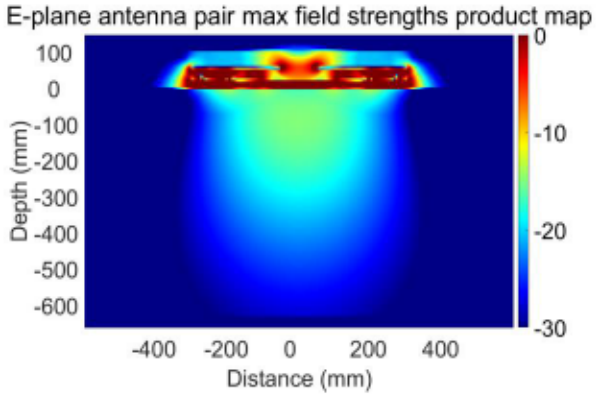

Fig. 9. Gopher antenna E-plane, combined radiation topography. Corresponds approximately to the 3dB 50° beamwidth at 0.6 m depth.

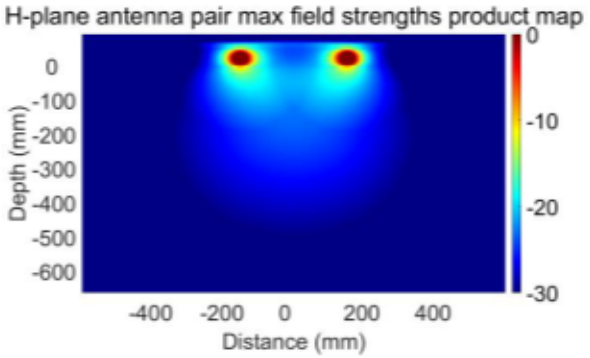

Fig. 10. Dipole antenna H-plane, combined radiation topography. Corresponds approximately to the 3dB 80° beamwidth at 0.6 m depth.

V. EFFECT OF THE PULSE WIDTH

The central frequency of these antennas in the air is below 500 MHz. Here a short Gaussian pulse of 0.47 ns is applied to see its effect to the radiation topography. The central frequency of the pulse spectrum is 1140 MHz, thus well above the central frequency of the antenna. The results are shown in Fig. 11 and Fig. 12.

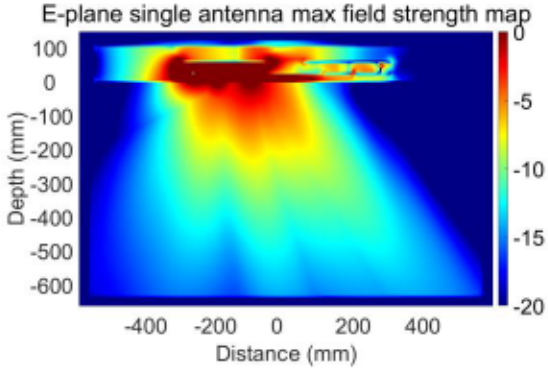

Fig. 11. A short Gaussian pulse of 0.47 ns with Gopher antenna E-plane (yz). E-Plane goes through the antenna center. Compare to 0.

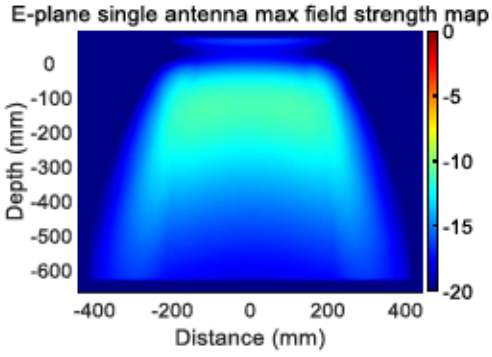

Fig. 12. A short Gaussian pulse of 0.47 ns with dipole antenna E-plane (xz). The E-plane is between antennas. Compare to Fig. 8.

The pulse pattern radiation topography visualization can be very beneficial for optimizing the pulse width for the desired purposes. A narrow beam as in Fig. 9 is good for point or line targets, like a pipeline in the sand. A reasonably wide beam is good for a synthetic aperture radar [2].

VI. CONVENTIONAL PULSE RADIATION VISUALIZATION APPLIED FOR THE GPR RANGE

In order to collect quantitative information of the radiating pulse, it is possible to record the field strength at defined points as a function of time. The pulse pattern for various angles at constant distance can be visualized using one or more of these: maximal cross-correlation (pulse fidelity factor), amplitude and spectrum. Variations of these can be seen in, e.g., [6] and [14]. Some visualization examples are further discussed below.

The amplitude of the electric field E_θ was calculated in the yz plane, perpendicular to the radius. The possible radial component was ignored as in [7]. The calculation results are shown in Table 1. It provides quantitative relative values on the pulse strength and quality in different directions at the constant distance of 300 mm.

The maximal normalized absolute cross-correlation depends on the pulse chosen for the comparison. In this case, the first derivative of the transmitted Gaussian pulse gave the highest results compared to the Gaussian or to the second derivative Gaussian pulse.

Table 1: Field values at 300 mm distance

Angle	240°	210°	180°	150°	120°
Max E field V/m	0.31	0.45	0.62	0.60	0.20
Max Cross-Correlation	0.80	0.85	0.93	0.94	0.95

Figure 13 shows the pulse versus time graphs in the same locations as in Table 1. The amplitude is easy to see, but the quality of the pulse is not easy to discern with the human eye. Figure 14 displays the same results with arrows. Line width is relative to the maximal power density at 300 mm from the antenna. Color is related to the maximal cross-correlation: lowest orange, highest cyan. One other possibility could be to show colored circles in the yz rectangular grid, the size of the circle relative to the power, and the circle color showing the quality.

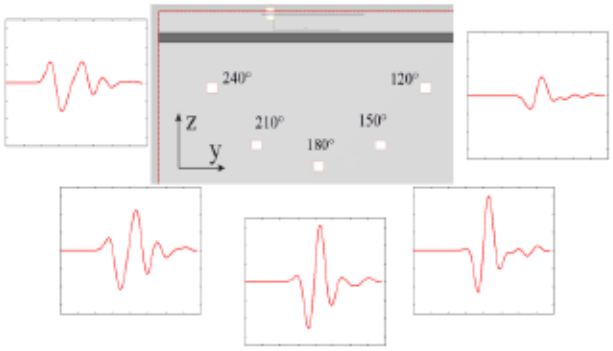

Fig. 13. Electric field versus time, yz plane, at 300 mm from the antenna. Simulation space section in the top center. Compare to 0.

Fig. 14. Field magnitude and pulse quality combined. Line width is relative to the maximal field magnitude at 300 mm from the antenna. The arrow orientations correspond to Fig. 13. Color is related to the maximal cross-correlation: lowest orange, highest cyan. Compare to Fig. 5. Data is from Table 1.

VII. COMPARISON WITH THE FAR FIELD NARROWBAND RADIATION PATTERNS

Figure 15 shows the far field pattern of the single Gopher antenna in narrowband frequencies in neoprene. Generally, it conforms with the pulse radiation topography. The maximal directivity and gain is 9.6 dBi at 0.4 GHz. Gain drops on upper and lower frequencies while directivity can be good.

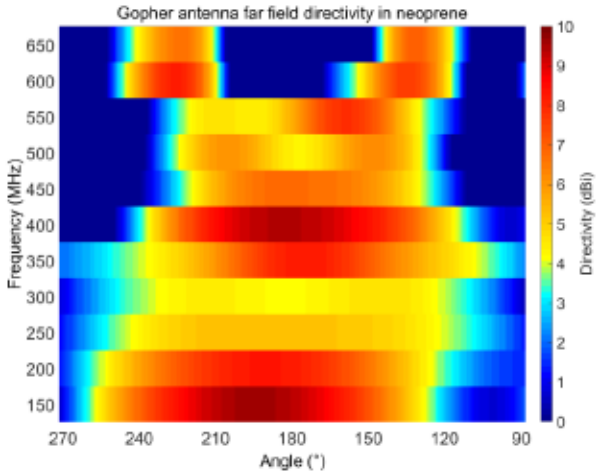

Fig. 15. Gopher antenna narrowband far field radiation pattern set: directivity D_ϑ versus frequency in the neoprene. $\varphi = 90°$, yz plane pattern. Angle ϑ corresponds to an antenna upside down towards the ground with the patch on the right side on the feed. 180° is downwards, 90° to the right, thus corresponding to the angles in Table 1 and in Figs. 13 and 14.

VIII. MEASURED PROFILE

Figure 16 is an example of a measured profile in a lake using the Gopher antenna. In the middle, there is a boat haven under the water. It is an approximately two meters wide trench where the bottom is approximately at one 0.8 m depth. Roundish stones are piled on both sides. In the profile the hyperbolas and the other artifacts are minimal, thus – although one cannot prove that – it can be considered implying a narrow beam or small radiation footprint. The radar pulse is 2 ns long and the permittivity of water $\varepsilon_r \approx 81$.

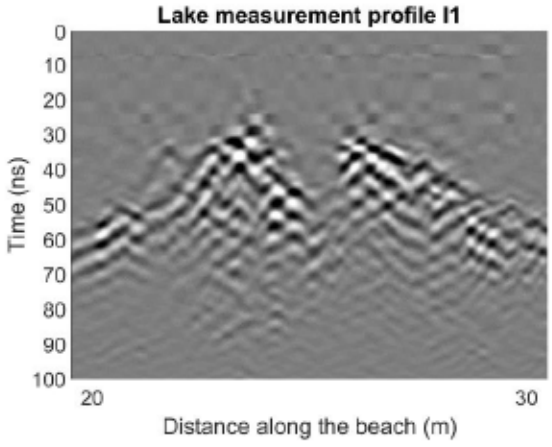

Fig. 16. Measured lake bottom profile crossing a boat haven submerged in the lake. It is an approximately two meters wide trench where the bottom is approximately at 0.8 m depth. Roundish stones are piled on both sides. Approximate horizontal distance values. 100 ns time corresponds to the depth approximately 1.6 m.

IX. EVALUATION OF THE FINDINGS AND CONCLUSION

Table 1 shows that to some directions the cross-correlation deteriorates with the strength of the pulse. It means that the explorative expectation mentioned in Section II does not strictly speaking hold. A low quality pulse shape means that the target is not recognizable even when the signal is strong. Quantifying the combination of these two properties of the pulse radiation is an important item for further study.

In this paper, I have proposed a new method to characterize GPR radiation in the ground: it stores the highest electric field magnitude during the FDTD simulation in each pixel in a defined plane. The method adds to the available tool set, although it can be utilized on its own. This visualization can be utilized effectively in the GPR antenna development. This method provides a new perspective for GPR antenna design, helps customize the transmit pulse and opens new opportunities for future research.

ACKNOWLEDGMENTS

At Aalto University: Research Engineer Matti Vaaja and Associate Professor Ville Viikari, and at Easy Radar USA Chief Engineer Karl Harrar.

REFERENCES

[1] D. Daniels, *Ground Penetrating Radar*. London: IET, 2004.

[2] D. Comite, A. Galli, I. Catapano, and F. Soldovieri, "The role of the antenna radiation pattern in the performance of a microwave tomographic approach for GPR imaging," *IEEE Journal of Selected Topics in Applied Earth Observations and Remote Sensing*, vol. 10, no. 10, pp. 4337-4347, Oct. 2017.

[3] H. Jol, *Ground Penetrating Radar: Theory and applications*. Oxford: Elsevier Science, 2009.

[4] C. Warren and A. Giannopoulos, "Characterisation of a ground penetrating radar antenna in lossless homogeneous and lossy heterogeneous environments," *Signal Processing*, vol. 132, no. Mar., pp. 221-226, Mar. 2017.

[5] C. Warren and A. Giannopoulos, "Experimental and modeled performance of a ground penetrating radar antenna in lossy dielectrics," *IEEE Journal of Selected Topics in Applied Earth Observations and Remote Sensing*, vol. 9, no. 1, pp. 29-36, Jan. 2016.

[6] H. Schantz, *The Art and Science of Ultrawideband Antennas*. 2nd edition, Boston: Artech House, 2015.

[7] N. Diamanti and A. P. Annan, "Characterizing the energy distribution around GPR antennas," *Journal of Applied Geophysics*, vol. 99, pp. 83-90, Dec.

2013.

[8] M. Hall, L. Barclay, and M. Hewitt, *Propagation of Radiowawes*. Exeter: Short Run Press, 1996.

[9] V.-E. Voipio, "The Gopher antenna - A new efficient design for ground penetrating radar," in *International Workshop on Advanced Ground Penetrating Radar*, Hague, Netherlands, pp. 1-5, Sep. 2019.

[10] L. Pajewski, A. Giannopoulos, C. Warren, S. Antonijevic, V. Doric, D. Poljac, and D. Pirrone, "Development of electromagnetic simulators for ground penetrating radar," in *2017 International Applied Computational Electromagnetics Society (ACES) Symposium*, Firenze, Italy, pp. 1-2, Mar. 2017.

[11] A. Elsherbeni and D. Veysel, *The Finite-Difference Time-Domain Method for Electromagnetics with MATLAB Simulations*. Raleigh NC: SciTech Publishing Inc., 2008.

[12] K. Holliger and T. Bergmann, "Accurate and efficient FDTD modeling of ground-penetrating radar radiation," *Geophysical Research Letters*, vol. 25, no. 20, pp. 3883-3886, Oct. 15, 1998.

[13] C. Warren and A. Giannopoulos, "Creating FDTD models of commercial GPR antennas using Taguchi's optimisation method," *Geophysics*, vol. 76, no. 2, pp. 37-47, Mar.-Apr. 2011.

[14] C. A. Balanis, *Modern Antenna Handbook*. Hoboken NJ: Wiley, 2008.